

The Beam–Charge Azimuthal Asymmetry and Deeply Virtual Compton Scattering

A. Airapetian,¹⁷ N. Akopov,²⁹ Z. Akopov,²⁹ M. Amarian,^{8,29} A. Andrus,¹⁶ E.C. Aschenauer,⁸ W. Augustyniak,²⁸ R. Avakian,²⁹ A. Avetissian,²⁹ E. Avetissian,¹² P. Bailey,¹⁶ D. Balin,²⁰ M. Beckmann,⁷ S. Belostotski,²⁰ N. Bianchi,¹² H.P. Blok,^{19,27} H. Böttcher,⁸ A. Borissov,¹⁵ A. Borysenko,¹² M. Bouwhuis,¹⁶ A. Brüll*, V. Bryzgalov,²¹ M. Capiluppi,¹¹ G.P. Capitani,¹² T. Chen,⁴ G. Ciullo,¹¹ M. Contalbrigo,¹¹ P.F. Dalpiaz,¹¹ W. Deconinck,¹⁷ R. De Leo,³ M. Demey,¹⁹ L. De Nardo,¹ E. De Sanctis,¹² E. Devitsin,¹⁸ P. Di Nezza,¹² J. Dreschler,¹⁹ M. Düren,¹⁴ M. Ehrenfried,¹⁰ A. Elalaoui-Moulay,² G. Elbakian,²⁹ F. Ellinghaus,⁶ U. Elschenbroich,¹³ R. Fabbri,¹⁹ A. Fantoni,¹² L. Felawka,²⁵ S. Frullani,²³ A. Funel,¹² G. Gapienko,²¹ V. Gapienko,²¹ F. Garibaldi,²³ K. Garrow,²⁵ D. Gaskell,⁶ G. Gavrilov,^{7,20,25} V. Gharibyan,²⁹ O. Grebeniouk,²⁰ I.M. Gregor,⁸ C. Hadjidakis,¹² K. Hafidi,² M. Hartig,¹⁴ D. Hasch,¹² W.H.A. Hesselink,^{19,27} A. Hillenbrand,¹⁰ M. Hoek,¹⁴ Y. Holler,⁷ B. Hommez,¹³ I. Hristova,⁸ G. Iarygin,⁹ A. Ivanilov,²¹ A. Izotov,²⁰ H.E. Jackson,² A. Jgoun,²⁰ R. Kaiser,¹⁵ E. Kinney,⁶ A. Kisselev,^{6,20} T. Kobayashi,²⁶ M. Kopytin,⁸ V. Korotkov,²¹ V. Kozlov,¹⁸ B. Krauss,¹⁰ V.G. Krivokhijine,⁹ L. Lagamba,³ L. Lapikás,¹⁹ A. Laziev,^{19,27} P. Lenisa,¹¹ P. Liebing,⁸ L.A. Linden-Levy,¹⁶ W. Lorenzon,¹⁷ H. Lu,⁵ J. Lu,²⁵ S. Lu,¹⁴ B.-Q. Ma,⁴ B. Maiheu,¹³ N.C.R. Makins,¹⁶ Y. Mao,⁴ B. Marianski,²⁸ H. Marukyan,²⁹ F. Masoli,¹¹ V. Mexner,¹⁹ N. Meyners,⁷ T. Michler,¹⁰ O. Mikloukho,²⁰ C.A. Miller,^{1,25} Y. Miyachi,²⁶ V. Muccifora,¹² M. Murray,¹⁵ A. Nagaitsev,⁹ E. Nappi,³ Y. Naryshkin,²⁰ M. Negodaev,⁸ W.-D. Nowak,⁸ K. Oganessyan,^{7,12} H. Ohsuga,²⁶ A. Osborne,¹⁵ N. Pickert,¹⁰ D.H. Potterveld,² M. Raithel,¹⁰ D. Reggiani,¹⁰ P.E. Reimer,² A. Reischl,¹⁹ A.R. Reolon,¹² C. Riedl,¹⁰ K. Rith,¹⁰ G. Rosner,¹⁵ A. Rostomyan,²⁹ L. Rubacek,¹⁴ J. Rubin,¹⁶ D. Ryckbosch,¹³ Y. Salomatin,²¹ I. Sanjiev,^{2,20} I. Savin,⁹ A. Schäfer,²² G. Schnell,²⁶ K.P. Schüler,⁷ J. Seele,⁶ R. Seidl,¹⁰ B. Seitz,¹⁴ R. Shanidze,¹⁰ C. Shearer,¹⁵ T.-A. Shibata,²⁶ V. Shutov,⁹ K. Sinram,⁷ W. Sommer,¹⁴ M. Stancari,¹¹ M. Statera,¹¹ E. Steffens,¹⁰ J.J.M. Steijger,¹⁹ H. Stenzel,¹⁴ J. Stewart,⁸ F. Stinzing,¹⁰ P. Tait,¹⁰ H. Tanaka,²⁶ S. Taroian,²⁹ B. Tchuiko,²¹ A. Terkulov,¹⁸ A. Trzcinski,²⁸ M. Tytgat,¹³ A. Vandenbroucke,¹³ P.B. van der Nat,¹⁹ G. van der Steenhoven,¹⁹ Y. van Haarlem,¹³ V. Vikhrov,²⁰ M.G. Vincter,¹ C. Vogel,¹⁰ J. Volmer,⁸ S. Wang,⁴ J. Wendland,^{24,25} Y. Ye,⁵ Z. Ye,⁷ S. Yen,²⁵ B. Zihlmann,¹³ and P. Zupranski²⁸

(The HERMES Collaboration)

¹Department of Physics, University of Alberta, Edmonton, Alberta T6G 2J1, Canada

²Physics Division, Argonne National Laboratory, Argonne, Illinois 60439-4843, USA

³Istituto Nazionale di Fisica Nucleare, Sezione di Bari, 70124 Bari, Italy

⁴School of Physics, Peking University, Beijing 100871, China

⁵Department of Modern Physics, University of Science and Technology of China, Hefei, Anhui 230026, China

⁶Nuclear Physics Laboratory, University of Colorado, Boulder, Colorado 80309-0390, USA

⁷DESY, 22603 Hamburg, Germany

⁸DESY, 15738 Zeuthen, Germany

⁹Joint Institute for Nuclear Research, 141980 Dubna, Russia

¹⁰Physikalisches Institut, Universität Erlangen-Nürnberg, 91058 Erlangen, Germany

¹¹Istituto Nazionale di Fisica Nucleare, Sezione di Ferrara and

Dipartimento di Fisica, Università di Ferrara, 44100 Ferrara, Italy

¹²Istituto Nazionale di Fisica Nucleare, Laboratori Nazionali di Frascati, 00044 Frascati, Italy

¹³Department of Subatomic and Radiation Physics, University of Gent, 9000 Gent, Belgium

¹⁴Physikalisch Institut, Universität Gießen, 35392 Gießen, Germany

¹⁵Department of Physics and Astronomy, University of Glasgow, Glasgow G12 8QQ, United Kingdom

¹⁶Department of Physics, University of Illinois, Urbana, Illinois 61801-3080, USA

¹⁷Randall Laboratory of Physics, University of Michigan, Ann Arbor, Michigan 48109-1040, USA

¹⁸Lebedev Physical Institute, 117924 Moscow, Russia

¹⁹Nationaal Instituut voor Kernfysica en Hoge-Energiefysica (NIKHEF), 1009 DB Amsterdam, The Netherlands

²⁰Petersburg Nuclear Physics Institute, St. Petersburg, Gatchina, 188350 Russia

²¹Institute for High Energy Physics, Protvino, Moscow region, 142281 Russia

²²Institut für Theoretische Physik, Universität Regensburg, 93040 Regensburg, Germany

²³Istituto Nazionale di Fisica Nucleare, Sezione Roma 1, Gruppo Sanità

and Physics Laboratory, Istituto Superiore di Sanità, 00161 Roma, Italy

²⁴Department of Physics, Simon Fraser University, Burnaby, British Columbia V5A 1S6, Canada

²⁵TRIUMF, Vancouver, British Columbia V6T 2A3, Canada

²⁶Department of Physics, Tokyo Institute of Technology, Tokyo 152, Japan

²⁷Department of Physics and Astronomy, Vrije Universiteit, 1081 HV Amsterdam, The Netherlands

²⁸Andrzej Soltan Institute for Nuclear Studies, 00-689 Warsaw, Poland

²⁹Yerevan Physics Institute, 375036 Yerevan, Armenia

(Dated: February 8, 2020)

The first observation of an azimuthal cross-section asymmetry with respect to the charge of the incoming lepton beam is reported from a study of hard exclusive electroproduction of real photons. The data have been accumulated by the HERMES experiment at DESY, in which the HERA 27.6 GeV electron or positron beam scattered off an unpolarized hydrogen gas target. The observed asymmetry is attributed to the interference between the Bethe–Heitler process and the Deeply Virtual Compton Scattering (DVCS) process. The interference term is sensitive to DVCS amplitudes, which provide the most direct access to Generalized Parton Distributions.

PACS numbers: 13.60.-r, 24.85.+p, 13.60.Fz, 14.20.Dh

The partonic structure of the nucleon has been traditionally described in terms of Parton Distribution Functions (PDFs), which appear in the interpretation of, e.g., inclusive Deeply Inelastic Scattering (DIS). More recently, PDFs have been subsumed within Generalized Parton Distributions (GPDs) [1, 2, 3], which relate directly to hard exclusive processes that involve at least one additional hard vertex, yet leave the target nucleon intact. The ordinary PDFs and nucleon elastic form factors appear as kinematic limits and moments of GPDs, respectively. Strong interest in the formalism of GPDs has emerged after GPDs were found to offer the first possibility to reveal the total angular momentum carried by the quarks in the nucleon [2]. More recent discussions focus on the potential of GPDs as a three-dimensional representation of hadrons at the parton level [4, 5, 6, 7].

Among all practical probes, the DVCS process, i.e., the hard exclusive lepton production of a real photon, appears to provide the theoretically cleanest access to GPDs. Direct access to the DVCS *amplitudes* is provided by the interference between the DVCS and Bethe–Heitler (BH) processes, in which the photon is radiated from a parton and from the lepton, respectively. Since these processes have an identical final state, their scattering amplitudes add coherently. The squared photon production amplitude is given by

$$|\tau|^2 = |\tau_{BH}|^2 + |\tau_{DVCS}|^2 + \underbrace{\tau_{DVCS} \tau_{BH}^* + \tau_{DVCS}^* \tau_{BH}}_I, \quad (1)$$

where I denotes the interference term. The BH amplitude (τ_{BH}) is precisely calculable from measured elastic form factors. For an unpolarized proton target, the cross section for exclusive lepton production of a real photon reads [8]

$$\frac{d^4\sigma}{dx_B dQ^2 d|t| d\phi} = \frac{x_B y^2}{32(2\pi)^4 Q^4} \frac{|\tau|^2}{\sqrt{1 + 4x_B^2 M_p^2/Q^2}}, \quad (2)$$

where x_B represents the Bjorken scaling variable, $-Q^2$ the squared virtual–photon four-momentum, y the fraction of the incident lepton energy carried by the virtual

photon in the target rest frame, M_p is the proton mass, and t is the square of the four-momentum transfer to the target. The above interpretation of the virtual–photon kinematics does not apply to the BH process. The azimuthal angle $\phi \in [-\pi, \pi]$ is defined as the angle between the plane containing the incoming and outgoing lepton trajectories and the plane correspondingly defined by the virtual and the real photon. The interference term is given by [8]

$$I = -C \frac{32(2\pi)^3 \sqrt{2} \alpha^3 M_p}{t Q x_B} \frac{1}{\sqrt{1-x_B}} \times \left[\cos \phi \frac{1}{\sqrt{\epsilon(1-\epsilon)}} \text{Re} \widetilde{\mathcal{M}}^{1,1} - P_l \sin \phi \sqrt{\frac{1+\epsilon}{\epsilon}} \text{Im} \widetilde{\mathcal{M}}^{1,1} \right], \quad (3)$$

where the lepton beam has a longitudinal polarization P_l and charge $C = \pm 1$, α denotes the electromagnetic coupling constant, and ϵ is the ratio of the longitudinal to transverse virtual–photon flux. A polarization-independent constant term as well as higher harmonics ($\cos 2\phi, \cos 3\phi, \sin 2\phi$) have been neglected in Eq. 3 since they are suppressed by at least $\mathcal{O}(1/Q)$ or $\mathcal{O}(\alpha_s)$, where α_s is the strong coupling constant. Whereas the squared BH and DVCS amplitudes do not depend on the sign of the charge, the measurement of a cross section asymmetry with respect to the beam charge can be used to isolate the real part of the interference term [9], while the imaginary part is accessible through an asymmetry with respect to the beam helicity [10]. The photon–helicity–conserving amplitude

$$\widetilde{\mathcal{M}}^{1,1} = F_1 \mathcal{H}_1 + \frac{x_B}{2-x_B} (F_1 + F_2) \widetilde{\mathcal{H}}_1 - \frac{t}{4M_p^2} F_2 \mathcal{E}_1 \quad (4)$$

is given by a linear combination of the Compton Form Factors (CFFs) $\mathcal{H}_1, \widetilde{\mathcal{H}}_1$ and \mathcal{E}_1 , together with the Dirac and Pauli form factors F_1 and F_2 [11]. The CFFs are convolutions of the corresponding twist–2 GPDs H, \widetilde{H} and E with the hard scattering amplitude.

The imaginary part of $\widetilde{\mathcal{M}}^{1,1}$ is manifest as a $\sin \phi$ modulation in azimuthal cross-section asymmetries with respect to the beam helicity, which already have been observed [12, 13]. This Letter reports the first measurement of an azimuthal asymmetry with respect to the beam charge, accessing the real part of $\widetilde{\mathcal{M}}^{1,1}$ via a $\cos \phi$ modulation.

*Present address: Thomas Jefferson National Accelerator Facility, Newport News, Virginia 23606, USA

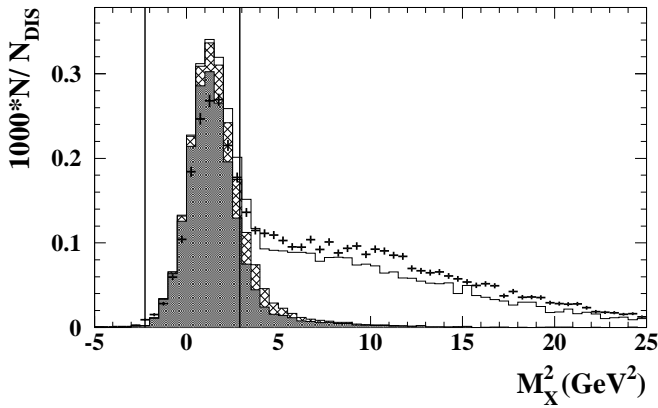


FIG. 1: Distributions in missing-mass squared from data (statistical error bars) and from Monte Carlo simulations (line). The latter include elastic BH (filled area) and associated BH (hatched area) processes as well as semi-inclusive background. The vertical lines enclose the selected exclusive region.

Data with an unpolarized hydrogen target were accumulated using the HERMES spectrometer [14] and the longitudinally polarized 27.6 GeV electron and positron beams of the HERA accelerator at DESY. Events were selected if they contained exactly one photon and one charged track identified as the scattered lepton. Leptons were distinguished from hadrons with an efficiency of 98% using the combined information from a transition-radiation detector, a preshower scintillator detector, and an electromagnetic calorimeter. The remaining hadron contamination in the lepton sample is smaller than 1%. The kinematic requirements imposed were $1 \text{ GeV}^2 < Q^2 < 10 \text{ GeV}^2$, $0.03 < x_B < 0.35$, $W > 3 \text{ GeV}$, and $\nu < 22 \text{ GeV}$, where W denotes the initial photon-nucleon invariant mass and ν is the virtual-photon energy in the target rest frame. The real photon was identified by detecting an energy deposition above 5 GeV in the calorimeter in addition to a signal in the preshower detector, without an associated charged track in the back region of the spectrometer. Unlike in a preliminary stage of this analysis [15], the useful range of the polar angle $\theta_{\gamma^*\gamma}$ between the virtual and real photons is not limited by the photon position resolution, due to an improved reconstruction algorithm. Now the restriction on $\theta_{\gamma^*\gamma}$ is relaxed to $\theta_{\gamma^*\gamma} > 5 \text{ mrad}$, limited mainly by the electron momentum resolution. In addition, a stricter upper limit of $\theta_{\gamma^*\gamma} < 45 \text{ mrad}$ is imposed in order to improve the signal-to-background ratio [16].

The recoiling proton was not detected. Hence exclusive events are selected by requiring the missing mass M_X of the reaction $ep \rightarrow e\gamma X$ to be close to the proton mass. Fig. 1 shows the distribution in $M_X^2 = (q+p-q')^2$, with q , p , and q' being the four-momenta of the virtual photon, the target nucleon in the initial state, and the real photon, respectively. Mainly due to the resolution in photon energy, the exclusive peak extends to negative values, in

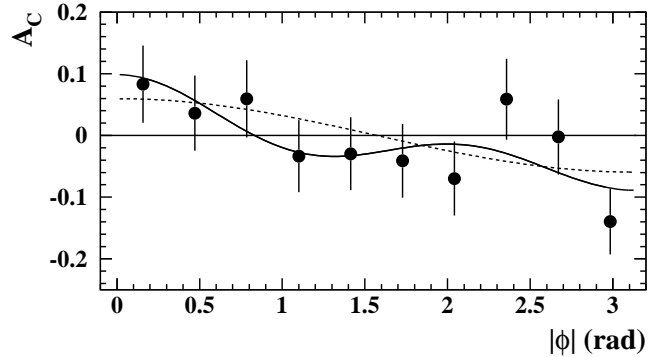


FIG. 2: Beam-charge asymmetry A_C for the hard electro-production of photons off protons as a function of the azimuthal angle $|\phi|$, for the exclusive sample before background correction. Statistical uncertainties are shown. The solid curve shows the result of a four-parameter fit: $(-0.011 \pm 0.019) + (0.060 \pm 0.027) \cos \phi + (0.016 \pm 0.026) \cos 2\phi + (0.034 \pm 0.027) \cos 3\phi$. The dashed line shows the pure $\cos \phi$ dependence.

which case M_X is defined as $-\sqrt{-M_X^2}$. The exclusive region is defined as $(-1.5 \text{ GeV})^2 < M_X^2 < (1.7 \text{ GeV})^2$, based on the result of a Monte Carlo simulation (MC), shown in the same figure. The Mo and Tsai formalism [20] is used to simulate the elastic BH process leaving the target nucleon intact, and the associated BH process, where the nucleon is excited to a resonant state. For the latter a cross-section parametrization for the resonance region is used [21]. Not included in the simulation is the DVCS contribution, which in this kinematic regime is expected to be much smaller than that of the BH process [22]. The simulation also takes into account the semi-inclusive production of neutral mesons (mostly π^0), where all but one of the decay photons escape detection. For this, the MC generator LEPTO [17] in conjunction with a special JETSET [18] fragmentation tune is used, the latter being optimized for energies relevant to HERMES [19]. As shown in Fig. 1, data and MC are in good agreement taking into account that they are both absolutely normalized, and that the MC does not include radiative corrections to the BH cross-section. The MC yield exceeds the data by about 20% in the exclusive region, as may be expected [24]. A simulation including second order radiative processes should give an improved MC-data comparison in the full missing mass region, since a part of the exclusive events experiencing second order radiative corrections will not be lost but reconstructed in the non-exclusive region.

The beam-charge asymmetry is evaluated as

$$A_C(\phi) = \frac{N^+(\phi) - N^-(\phi)}{N^+(\phi) + N^-(\phi)}, \quad (5)$$

where $N^+(\phi)$ and $N^-(\phi)$ represent the single-photon yields per ϕ bin, normalized to the number of detected inclusive DIS events using the positron and electron beam,

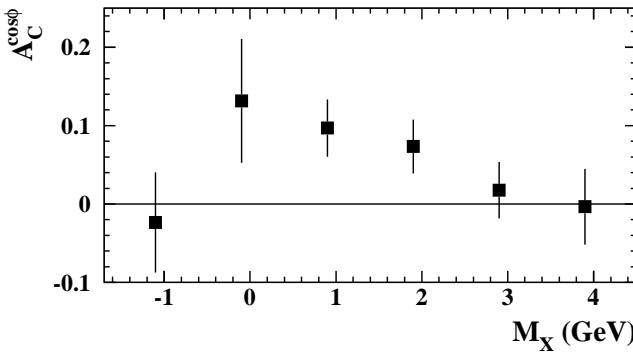


FIG. 3: The $\cos \phi$ amplitude of the beam–charge asymmetry as a function of the missing mass. Statistical uncertainties are shown.

respectively. Since these beams were polarized, sinusoidal contributions appear in numerator and denominator of Eq. 5, with the last term in Eq. 3 giving the biggest contribution. In order to cancel these contributions, the ‘symmetrized’ beam–charge asymmetry is calculated by replacing ϕ by $|\phi|$ in Eq. 5. The result for the exclusive region is displayed in Fig. 2. The shown four–parameter fit yields a non-zero $\cos \phi$ amplitude of 0.060 ± 0.027 . The result after the background correction described below is given in Table I, last row. The constant term as well as the $\cos 2\phi$ and $\cos 3\phi$ terms are compatible with zero. At higher missing masses, the $\cos \phi$ dependence of the beam–charge asymmetry is compatible with zero as can be seen in Fig. 3, where the results of the fit carried out in several missing mass bins are shown.

As the recoiling proton remains undetected, t is inferred from the measurement of the other final–state particles. For elastic events, kinematics relate the energy with the direction of the real photon, opening the possibility to omit the real–photon energy, which is the quantity subject to larger uncertainty. Thus the value of t in the exclusive region is calculated as

$$t = \frac{-Q^2 - 2\nu(\nu - \sqrt{\nu^2 + Q^2} \cos \theta_{\gamma^*\gamma})}{1 + \frac{1}{M_p}(\nu - \sqrt{\nu^2 + Q^2} \cos \theta_{\gamma^*\gamma})}. \quad (6)$$

The error caused by applying this expression to inelastic events ($\approx 17\%$ in the exclusive region) is accounted for in the MC simulation that is used to calculate the fractional contribution of background processes per kinematic bin in $-t$ (see Ref. [16] for details).

Figure 4 shows the $\cos \phi$ amplitude derived from the four–parameter fit in each of four bins in $-t$. In each bin, this result is corrected for the beam–charge–independent dilution by the semi–inclusive background in the exclusive region, which is about 6% in total. It is derived from the MC simulation described above, wherein the elastic and associated BH contributions are scaled down by the 20% by which the MC exceeds the data in the exclusive region. The uncertainty on the background contributions

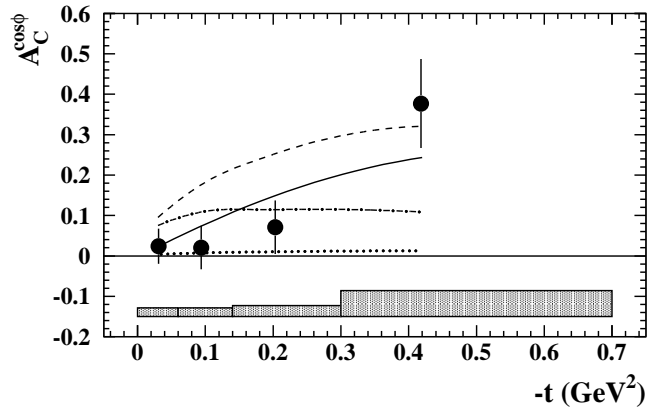


FIG. 4: The $\cos \phi$ amplitude of the beam–charge asymmetry as a function of $-t$ for the exclusive region ($-1.5 \text{ GeV} < M_X < 1.7 \text{ GeV}$), after background correction. The error bars (band) represent(s) the statistical (systematic) uncertainties. The calculations based on GPD models [25, 26] use either a factorized t –dependence with (dashed–dotted) or without (dotted) the D–term contribution, or a Regge–inspired t –dependence with (dashed) or without (solid) the D–term contribution.

per bin is taken into account in the total systematic uncertainty. After this correction, the resulting $\cos \phi$ amplitudes are expected to originate from only elastic and associated production. The associated BH processes contribute about 5, 11, 18, and 29% to the yields in the four $-t$ bins, or 11% in the full t –range, with an estimated fractional uncertainty of 10%. The dominant contribution to the total systematic uncertainty of the $\cos \phi$ amplitudes stems from effects due to possible deviations of the detector and/or the beam from their nominal positions. These effects can be as large as 0.02 per bin. Smearing effects can contribute up to 15% of the $\cos \phi$ amplitude and thus dominate the systematic uncertainty in the last $-t$ bin. The other sources of systematic uncertainties are due to a possible difference in the calorimeter calibration between the two data sets, the remaining uncertainties from the semi–inclusive background correction as described above, and the dilution of the asymmetry due to exclusively produced π^0 mesons misidentified as photons. These contributions are combined quadratically in the total systematic uncertainty per bin in $-t$, given in Table I¹. Not included is any contribution due to additional QED vertices, as the most significant of these has been estimated to be negligible, at least in the case of polarization asymmetries [23].

¹ Note that a preliminary result of this analysis [15] with a t –averaged value of 0.11 ± 0.04 (stat.) ± 0.03 (sys.) was derived at a much larger mean $-t$ value ($\langle -t \rangle = 0.27 \text{ GeV}^2$) due to different requirements on $\theta_{\gamma^*\gamma}$, as described above. It thus cannot be compared to the t –averaged result given in Table I but approximately to the result in the third $-t$ bin.

$-t$ bin (GeV^2)	$\langle -t \rangle$ (GeV^2)	$\langle x_B \rangle$	$\langle Q^2 \rangle$ (GeV^2)	$A_C^{\cos \phi} \pm \text{stat.} \pm \text{sys.}$
0.00 – 0.06	0.03	0.08	2.0	$0.024 \pm 0.043 \pm 0.021$
0.06 – 0.14	0.09	0.10	2.6	$0.020 \pm 0.054 \pm 0.022$
0.14 – 0.30	0.20	0.11	3.0	$0.071 \pm 0.066 \pm 0.027$
0.30 – 0.70	0.42	0.12	3.7	$0.377 \pm 0.110 \pm 0.064$
0.00 – 0.70	0.12	0.10	2.5	$0.063 \pm 0.029 \pm 0.026$

TABLE I: The $\cos \phi$ amplitude of the beam–charge asymmetry per kinematic bin in $-t$ after background correction and the respective average kinematic values.

The theoretical calculations for the $e p \rightarrow e p \gamma$ process shown in Fig. 4 are based on GPD models developed in Refs. [25, 26]. The only model parameters of interest are those that change the GPD H since the impact of the GPDs \tilde{H} and E is suppressed at small values of x_B and $-t$, respectively (cf. Eq. 4). The code of Ref. [27] was used to calculate the values for the $\cos \phi$ amplitude of the beam–charge asymmetry at the average kinematics (see Table I) of every $-t$ bin and not at the kinematics of every event since it is too computationally intensive. The difference between these two approaches is strongly model dependent: Tests [28] show differences of up to 20% using the models in Ref. [22], which are equivalent to the factorized models in Fig. 4. Four different parameter sets are selected by choosing either a factorized or a Regge–inspired t –dependence, each with or without the contribution of the so–called D-term [29], which is related to the spontaneous breaking of chiral symmetry in QCD [26]. The parameters b_{val} and b_{sea} in the profile function [30] are fixed at unity, since the beam–charge asymmetry has been shown to be largely insensitive to them [16]. In comparing the predictions to the data, it should be borne in mind that the bin at largest $-t$ is subject to the largest contribution from associated production, which is not included in the model calculations. It may be considered remarkable that these GPD models developed in anticipation of the data are found to be reasonably successful. The data appear to disfavor the model based on the Regge–inspired t –dependence with the D-term contribution, especially when neglecting the bin at largest $-t$ for the reason given above. It is encouraging that measurements such as this can constrain the GPD H , even though the e^- integrated luminosity was only about 10 pb^{-1} .

In conclusion, a beam–charge azimuthal asymmetry in electroproduction of real photons has been measured for the first time. A $\cos \phi$ dependence has been observed in a kinematic region where the target proton is predominantly left intact. The $\cos \phi$ dependence is predicted to arise from the interference between the deeply virtual Compton scattering and Bethe–Heitler processes. These

initial data can already be used to distinguish among theoretical models for generalized parton distributions.

We gratefully acknowledge the DESY management for its support, the staff at DESY and the collaborating institutions for their significant effort, and our national funding agencies for financial support.

- [1] D. Müller et al., *Fortschr. Phys.* **42** (1994) 101.
- [2] X. Ji, *Phys. Rev. Lett.* **78** (1997) 610; X. Ji, *Phys. Rev.* **D55** (1997) 7114.
- [3] A.V. Radyushkin, *Phys. Rev.* **D56** (1997) 5524.
- [4] M. Burkhardt, *Phys. Rev.* **D62** (2000) 071503; Erratum–ibid. **D 66** (2002) 119903.
- [5] M. Diehl, *Eur. Phys. J.* **C25** (2002) 223; Erratum–ibid. **C31** (2003) 277.
- [6] J.P. Ralston and B. Pire, *Phys. Rev.* **D66** (2002) 111501.
- [7] M. Burkhardt, *Int. J. Mod. Phys.* **A18** (2003) 173.
- [8] M. Diehl et al., *Phys. Lett.* **B411** (1997) 193.
- [9] S.J. Brodsky, F.E. Close and J.F. Gunion, *Phys. Rev.* **D6** (1972) 177.
- [10] P. Kroll, M. Schürmann and P.A.M. Guichon, *Nucl. Phys.* **A598** (1996) 435.
- [11] A.V. Belitsky, D. Müller and A. Kirchner, *Nucl. Phys.* **B629** (2002) 323.
- [12] HERMES Collaboration, A. Airapetian et al., *Phys. Rev. Lett.* **87** (2001) 182001.
- [13] CLAS Collaboration, S. Stepanyan et al., *Phys. Rev. Lett.* **87** (2001) 182002.
- [14] HERMES Collaboration, K. Ackerstaff et al., *Nucl. Instr. and Meth.* **A417** (1998) 230.
- [15] F. Ellinghaus (for the HERMES Collaboration), *Nucl. Phys.* **A711** (2002) 171.
- [16] F. Ellinghaus, PhD thesis, Humboldt University Berlin, Germany, January 2004, DESY-THESIS-2004-005.
- [17] G. Ingelman, A. Edin and J. Rathsman, *Comput. Phys. Commun.* **101** (1997) 108.
- [18] T. Sjöstrand, *Comput. Phys. Commun.* **82** (1994) 74.
- [19] A. Hillenbrand (for the HERMES Collaboration), *Proceedings of the 11th International Workshop on Deep–Inelastic Scattering*, St. Petersburg, Russia, April 2003.
- [20] L.W. Mo and Y.S. Tsai, *Rev. Mod. Phys.* **41** (1969) 205.
- [21] F.W. Brasse et al., *Nucl. Phys.* **B110** (1976) 413.
- [22] V.A. Korotkov and W.-D. Nowak, *Eur. Phys. J.* **C23** (2002) 455.
- [23] A.V. Afanasev, M.I. Konchatnij and N.P. Merenkov, [hep-ph/0507059](https://arxiv.org/abs/hep-ph/0507059).
- [24] M. Vanderhaeghen et al., *Phys. Rev.* **C62** (2000) 025501.
- [25] M. Vanderhaeghen, P.A.M. Guichon and M. Guidal, *Phys. Rev.* **D60** (1999) 094017.
- [26] K. Goeke, M.V. Polyakov and M. Vanderhaeghen, *Prog. Part. Nucl. Phys.* **47** (2001) 401.
- [27] M. Vanderhaeghen, P.A.M. Guichon and M. Guidal, Computer code for the calculation of DVCS and BH processes in the reaction $e p \rightarrow e p \gamma$, Priv. Comm., 2001.
- [28] B. Krauss, PhD thesis, University Erlangen–Nuremberg, Germany, February 2005, DESY-THESIS-2005-008.
- [29] M.V. Polyakov and C. Weiss, *Phys. Rev.* **D60** (1999) 114017.
- [30] I.V. Musatov and A.V. Radyushkin *Phys. Rev.* **D61** (2000) 074027.